23rd ABCM International Congress of Mechanical Engineering
December 6-11, 2015, Rio de Janeiro, RJ, Brazil

PROPOSITION OF A ROAD PROFILE IN SINE SHAPE TO STUDY FATIGUE LIFE OF VEHICLE SUSPENSION COMPONENTS

Luciano de Paula Rodrigues
Rita de Cássia Silva
University of Brasilia – UnB Gama College
Área Especial de Indústria Projeção A – UnB, Setor Leste
CEP: 72.444-240 Gama, Brazil
luciano.de.paula@hotmail.com
ritasilva@unb.br

Alessandro B. de S. Oliveira
University of Brasilia – UnB Gama College
Área Especial de Indústria Projeção A – UnB, Setor Leste
CEP: 72.444-240 Gama, Brazil
abso@unb.br

Abstract. *It is expected that paved surfaces to develop ruts with time. However even newly paved surfaces can present great roughness caused by inadequate paving process, for example. The interaction between suspension and road generates dynamic forces, which affect both the suspension and the pavement roughness. Vehicles can experience a broad spectrum of vibrations when travelling in roads and, the roughness of a road surface may be described by longitudinal profiles. The international roughness index – IRI represents a numerical scale for pavement roughness. In this work, IRI will be determined to an experimental road profile obtained from the CARSIM® software. An equivalent sinusoidal road profile will be proposed in a manner that its IRI is as near as possible of the experimental road profile. The amplitude and frequency in the sine function is established to provide this equivalence. Then a fatigue analysis is carried out using this sine-shaped profile to determine the SN curve to the control arms of a front Double "A" suspension. Preliminary results indicate that the methodology leads to a good agreement between the SN curves. Sine-shaped road profiles are simpler to reproduce in experimental tests and numerical analyses in order to study fatigue life.*

Keywords: *road profile, fatigue analysis, Method of Elements Finite, double wishbone, control arms, IRI*

1. INTRODUCTION

The interaction between vehicle suspension and road generates dynamic forces, which affect both the suspension subsystem (Gillespie, 1992) and the pavement roughness. The rougher the road, the greater the dynamic force exciting the suspension subsystem and, consequently causing more roughness. Vehicles can travel in roads at variable speed; hence, they experience a broad spectrum of vibrations (Gillespie, 1992) and, usually, the roughness of a road surface may be described by longitudinal profiles, which represent their elevation. According to Sayers (1998) longitudinal profiles cover texture, design grade and roughness.

In a vehicle, the suspension subsystem stands out as an important subsystem, because one of its main functions is to get the best out of the friction force between the tires and the road surface. Physically, this force guarantees steering control and, consequently, good handling (Gillespie, 1992).

Among the suspension vehicle components, the control arms have a relevant function, they can be found on almost every vehicle and they connect the knuckle to the chassis or sub-frame allowing steering knuckle to follow the wheel travel. The "A" arm are used in a suspension system called double wishbone suspension or double "A" suspension. It attaches the suspension on the chassis, but both controls arms have different roles. The upper transverse arm resists driving and braking torques and, the lower control arms pivot provides the wheel stroke. Reimpell, 2001 affirms, "*control arms ensure the desired kinematic behaviour of the rebounding and jouncing wheels and also transfer the wheel loadings to the body*". One of these forces is the lateral force, which generates a moment influenced by the control arms arrangement. This moment can increase the rolling effect of the body during cornering. Besides, the positions of the transverse arms relative to one another determine the height of the body roll centre, which directly influences in the stability of the vehicle.

As said, vehicle suspension suffers vibrations caused by unevenness surfaces provoked by the differences in quality of the road surface and by different velocities. A recognized manner to describe and classify the pavement quality in its longitudinal direction is the international roughness index – IRI (COTO, 2007; Chang *et al*, 2009; Santos, 2012). In addition, Finite Element Analysis (FEA) based on stress analysis has been applied to study fatigue life of this component considering typical loads, as that caused by the pavement irregularities, see section 3.

Thus, considering the relevance of the control arm component in a double wishbone suspension and, the IRI concept, in this work, an equivalent sinusoidal road profile, called theoretical road profile (TRP), will be proposed in a manner that its roughness index is as near as possible of an experimental road profile's (ERP) IRI. For this, the IRI index will be determined to an ERP obtained from the CARSIM® software and after, the amplitude and frequency in the sine function (TRP) will be established to provide this equivalence. Then the SN curves for both profiles ERP and TRP will be determined to the control arms of a front Double "A" suspension. Actually, the main purpose of this work is to propose a sinusoidal load profile, which is simpler to reproduce in fatigue experimental tests than a random profile, like that extracted from CARSIM® commercial software.

2. MODEL DESCRIPTION

The front double wishbone suspension treated at this work consists of two control arms, lower and upper, attached to the chassis and knuckle. The CAD model developed in CATIA VR5® was exported to the commercial software Autodesk Multiphysics® to be analyzed using finite elements (MEF).

To mesh both control arms solid elements are applied considering a cubic geometry with eight nodes. This choice is based on a sensibility study, which has shown good convergence and a lower runtime processing. The material specified to the control arms was the SAE 1020 HR. According to the sensibility study, the characteristics of the control arms' mesh can be summarized in Tab. 1. Figure 1 depicts the final mesh defined to the vehicle components.

Table 1. Mesh characteristics of the upper and lower control arms using Autodesk Multiphysics®

Mesh Characteristics	Lower Control arm	Upper Control Arm
Size of elements (mm)	2.24	3.95
Number of elements	17,322	11,222
Number of nodes	17,156	8,925

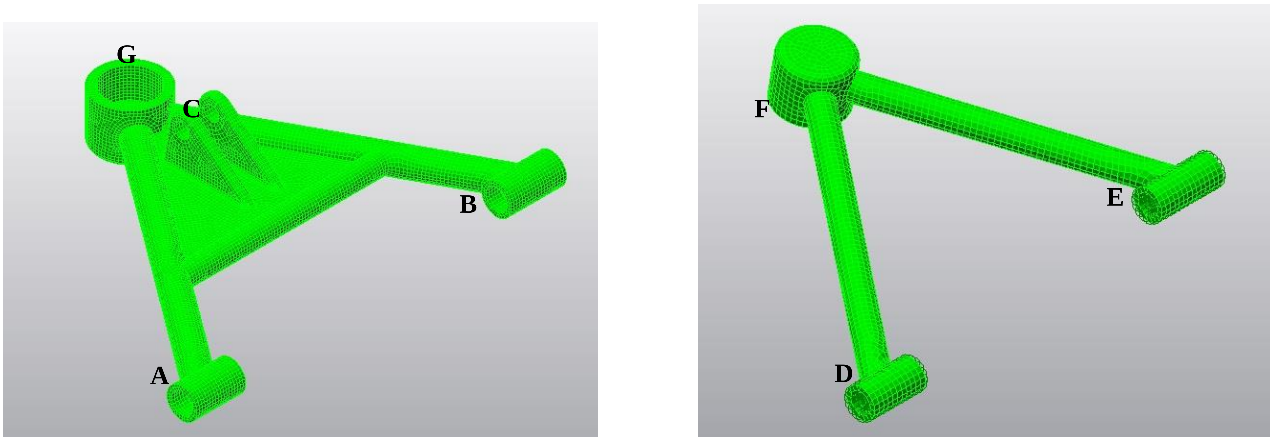

(a) (b)

Figure 1. Meshed vehicle components (a) lower control arm (b) upper control arm

The boundary conditions adopted to the model refers to the points A, B, C, D and E shown in Fig. 1. At these points only rotation is allowable, i.e., the degree of freedom concerning the translation are limited. The boundary conditions allow the wheels to travel around a bound and rebound limit (wheel travel). The forces considered in the model are applied at points F and G, as shown in Fig.1 (a) and (b).

3. DEFINITION OF INPUT DATA FOR FATIGUE ANALYSIS

This section presents the input data to be furnished to the commercial software Autodesk Simulation Multiphysics®, in order to develop the fatigue analysis obtaining the S-N curves of the control arms of the suspension vehicle. First, it is discussed how the forces acting in lower and upper control arms are defined. Notice that these forces correspond to a stress state of 90% of de ultimate tensile strength of the steel used in both components. Then it is presented the load profile to be follow that guarantee cyclic loads.

3.1 Fatigue strength: stress for one cycle life

Fatigue failure could be defined as the damage and failure of materials under cyclic loads (Suresh, 1998 and Shigley, 2008). A current condition can frequently happen, i.e., the stresses can vary with time or they can fluctuate between different levels thus, components can failed under the action of repeated or fluctuating stresses. Further analyses have shown that the actual maximum stresses of such a component are below the ultimate material's strength and generally below the yield strength.

In addition, it is noticed that a great part of static failures of components made of ductil materials develop a large deflection, when the stress level has exceeded the yield strength. Thus, such a situation provides a visible warning of failure, but in fatigue no signs are given and, generally, it is sudden and total.

In the automotive domain, the vehicle lifetime is highly determined by the fatigue life of its components. Such scenario leads the automotive industries to dedicate special attention to improve product quality and reliability to avoid early fatigue failure. For this, industries have invested in experimental or numerical methodologies that improve product considering this effect (Fourlaris *et al*, 2006; D'Ippolito *et al*, 2008; Zografos *et al*, 2009; Song and Lee, 2010; Ren *et al*, 2012).

In a typical *S-N* graph, there are two regions. The first one refers to low-cycle fatigue, which extends from stress cycle equals to one ($N = 1$) to $N = 10^3$ cycles. The second region, called high-cycle fatigue, refers to failure relative to stress cycles greater than this value (10^3 cycles). For steels, as hot-rolled (HR) SAE 1020 steel applied in the upper and lower control arms of the double wishbone suspension of the present work, it will be assumed that the boundary between finite-life and an infinite-life occurs at 10^6 cycles.

In addition, in the present study, the stress-life method will be applied in the fatigue analysis. As described by Shigley (2008) this method *"… is based on stress levels only, it is the least accurate approach, especially for low-cycle applications. However, it is the most traditional method, since it is the easiest to implement for a wide range of design applications, has ample supporting data, and represents high-cycle applications adequately."* Actually, despite the strain-life method be more adequate for low-cycle fatigue analysis, the stress-life method was chosen for the reasons described above, specially its good performance in high-cycle analysis. The construction of the *S-N* diagram for the stress-life method is presented in Shigley (2008).

It is noticed that in the low-cycle region the fatigue strength, S_f, has values very close to those of the ultimate tensile strength, S_{ut}. Generally, according to Shigley (2008) the specimen fatigue strength at 10^3 cycles can be defined as shown in Eq. (1):

$$\left(S'_f\right)_{10^3} = f\, S_{ut} \tag{1}$$

where factor f represents a fraction or percentage of the ultimate tensile strength, S_{ut} . In this paper, for HR SAE 1020 steel the ultimate tensile strength is adopted equals to 441 MPa (available in the *Autodesk Multiphysics*® material properties library*)*, hence, assuming a conservative value, f is taken equal to 0.9. This value is valid for steels with S_{ut} lower than 490 MPa (Shigley, 2008).

The forces necessary to achieve a stress state corresponding to 90% of the S_{ut} , Eq. (1), is 3700 N for the lower control arm and 2700 N for the upper control arm applied at point F and point G on the Fig. 1. It is important to highlight that those values of force correspond to cycle life equals to one ($N = 10^0 = 1$).

The fatigue simulation of both control arms is carried out with the commercial software Autodesk Simulation Multiphysics® using fatigue wizard tool. To determine the endurance limit, Autodesk Simulation Multiphysics® asks for the user the values of the multiplicative factors considered in the Marin equation (Shigley, 2008) and, in this paper, only the miscellaneous-effects modification factor, k_f, is taken into account.

3.2 Determining the load profile

As discussed in section 1 the main purpose of this paper is to present a theoretical road profile (TRP) to analyze fatigue life of vehicle suspension components. This way, it is proposed a double sine function, Eq. (2), which describes the load profile acting in the suspension vehicle.

$$y = A_1 \sin(w_1 t) + A_2 \cos(w_2 t) \tag{2}$$

where A_1 and A_2 are the amplitudes and w_1 and w_2 the frequencies.

The design variables are the amplitude (A_i) and the frequency (w_i), i assuming the values 1 and 2. For this, a random road profile is considered; the concepts involving the IRI are taken into account and simple statistical concepts are applied as will be explained throughout this section.

It is expected that paved surfaces to develop ruts with time, mainly provoked by the traffic of heavy vehicles. However even newly paved surfaces can present great roughness caused by inadequate paving process, poor materials and lack of a careful quality control. For ASTM E 867-82 pavement roughness is: "*the deviations of a surface from a true planar surface with characteristics dimensions that affect vehicle dynamics, ride quality, dynamic loads and* *drainage*". The DNER PRO 164/94 presents a definition very similar to that presented in the ASTM E 867-82, excluding only the effect of the drainage.

The IRI (ASTM E 1926-98 and ASTM E 1364-95) represents a numerical scale for pavement roughness based on the response of a ¼ vehicle model exposed to the roughness of the road surface, it varies from 0 (zero) to greater than 10, as shown in Tab. 2. In general, it represents a numerical value that expresses the accumulation of the millimeters of vertical movement of a quarter car. Besides, it can be cited as the most used roughness index for characterizing a pavement quality (COTO, 2007; Chang *et al*, 2009; Santos, 2012). It is important to highlight that the author proposes the first column, in order to facilitate the identification of the characteristics related to the IRI's values.

Table 2. Scale for the IRI index for paved roads with asphaltic concrete (adapted from ASTM E 1926-98)

Class	**IRI's values (m/km)**	**Characteristics**
1	0 - 3	Ride comfortable over 120 km/h. Depressions lower than 2 mm/3m. Typical high quality asphalt 1.4 to 2.3, high quality surface treatment 2.0 to 3.0.
2	3 - 6	Ride comfortable up to 100 – 120 km/h. Defective surface occasional depressions, patches or potholes (15 mm/3m or 10 -20 mm/5m). Surface without defects; moderate corrugations or large undulations.
3	6 - 8	Ride comfortable up to 70 – 90 km/h, strongly perceptible movements and swaying. Usually associated with defects; frequent moderate and uneven depressions or patches (e. g. 15 – 20 mm/3 m or 20 – 40 mm/5 m with frequency 5 – 3 per 50 m. Strong undulations or corrugations.
4	8 - 10	Ride comfortable up to 50 – 60 km/h, frequent sharp movements or swaying. Associated with severe defects; frequent deep and uneven depressions and patches (e. g. 20 -40 mm/3 m or 40 – 80 mm/5 m with frequency 5 – 3 per 5 m) or frequent potholes (e. g. 4 – 6 per 50 m).
5	Greater than 10	Necessary to reduce velocity below 50 km/h. Many deep depressions, potholes and severe disintegration (e. g. 40 -80 mm deep with frequency 8 – 16 per 50 m).

In addition, the suspension subsystem of a vehicle is designed to avoid an excessive vibration to be transmitted to the cabin compartment (Gillespie, 1995). At this context, the commercial software CarSim® and Proval® are used to help in the proposition of a TRP consisting in a double sine function, Eq. (2), which is applied in the fatigue analysis of the control arms (upper and lower) of a front double "A" suspension.

The CarSim® major proposal is to simulate dynamic behavior of vehicles. Profile Viewing and Analysis - Proval® (Chang *et al*, 2009) is an engineering software used to view and analyze pavement profiles.

3.2.1 Defining the amplitude of the double sine function

In this paper, a road profile named 101 is extracted from CarSim® road profile library. It acts in the left and right wheels during a vehicle simulation. Figure 2 depicts this road profile, which is called ERP. The amplitudes of the road unevenness are recorded about 140 s. As said in section 3.1, the fatigue analysis considers the damage provoked by cyclic loads, consequently, to define a function that establishes how the load acts to cause the fatigue effect is important.

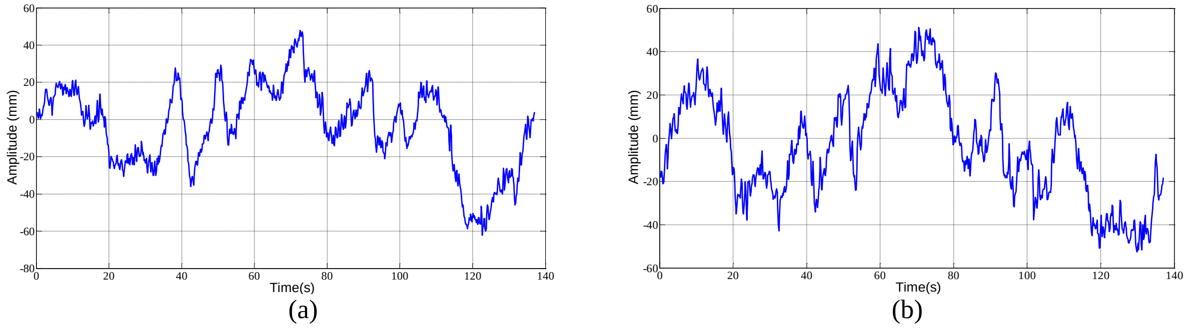

(a) (b)

Figure 2. Experimental Road Profile (EPR) extracted from CarSim® (a) left side (b) right side

The load illustrated at Fig. 2 is called as *Variable Amplitude Loading* and it is made up of many individual constant amplitude cycles. In addition, these individual cycles can each have different amplitude and mean, and at this case be superimposed. Each road profile have about 15 cycles.

In both sides of the road profile (Fig. 2), histograms are plotted to group the amplitudes of the road profile into logical bins as depicted by Fig. 3. The red line in the figures indicates the average value of the range with the highest occurrence. In Fig. 3 (a) the amplitude value is 12.05 mm and in Fig. 3 (b) it is -8.53 mm. The amplitudes, which correspond to the highest frequency, have opposite signs, in Fig. 3 (a) and (b). It means that, during the wheel stroke, the left wheel describe a bounce, while the right one a rebound.

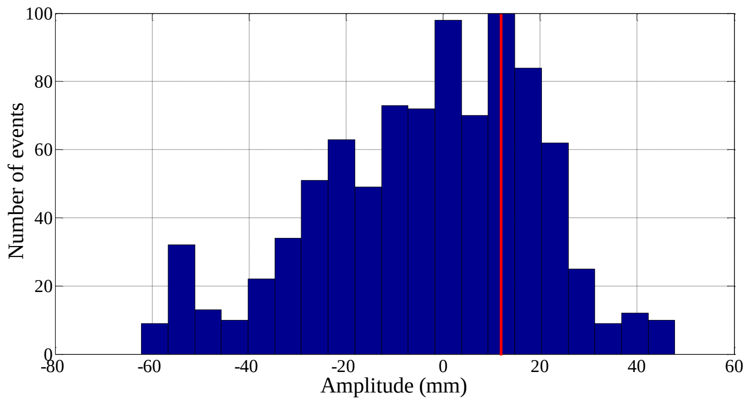

(a)

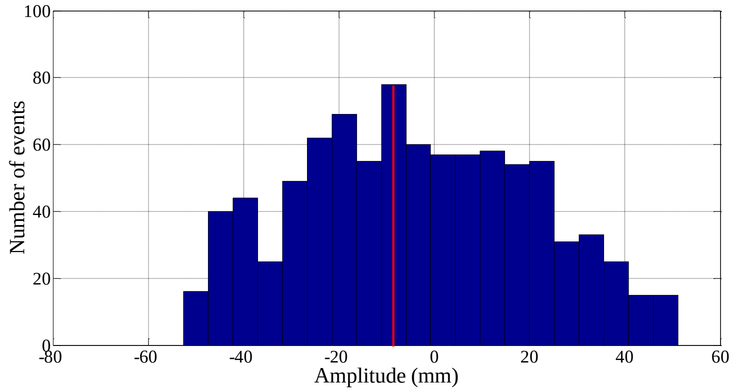

(b)

Figure 3. Histogram of EPR (a) left side (b) right side

3.2.2 The use of the IRI index to define the double sine function

To define the frequency of the double sine function, Eq. (2), the first approach was a spectral analysis of the load profile signs depicted in Fig. 2 (a) and (b); however, it was inconclusive. This way, another approach was to use IRI index to help determine the TPR. The Proval® software has been used to compute the IRI concerning the ERP, Fig. 2 (a) and (b) and thus, to classify the profile according to Tab. 2.

The data for the ERP is about 900 points for each side, Fig. 2 (a) and (b). Nevertheless, to use Proval® the data sample shall be divided into smaller samples. The flowchart below, Fig. 4, depicts how the total sample should be treated to furnish a representative IRI index.

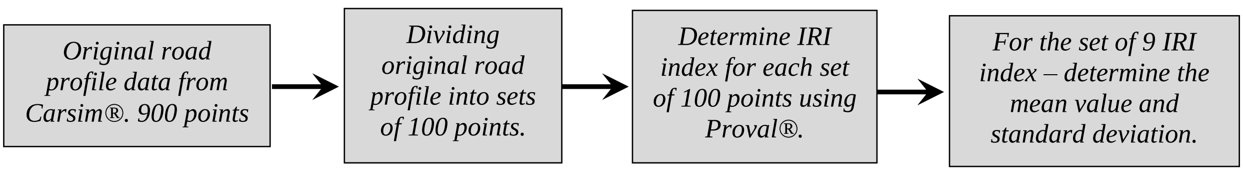

Figure 4. Methodology adopted to define the IRI index for each road profile

Following this methodology, the statistical values are expressed as (μ ± σ) and then, defined for the left ERP as 5.72 ± 0.74 m/km (class 2 according to Tab. 2) and, for the right side 6.77 ± 0.55 m/km (class 3 from Tab. 2). The values 5.72 and 6.72 m/km represent the average value, μ, and 0.74 and 0.55 m/km represent the standard deviation, σ.

Assuming A_1 and A_2 in Eq. (2) equal to 12.05 mm and the frequency, w_2, of the cosines term in Eq. (2) equals to 30% of the frequency w_1 of the sine term, it is possible to define the TRP in Eq. (3) for the left side. At this point, the main purpose was to define a load profile equation, which gives an IRI index close to the values found to the ERP. This way, the values of frequency varies from $(0.3:0.01:0.4)$ to the sine function in Eq. (2) and, from $0.3*(0.3:0.01:0.4)$ to the cosines, where 0.01 is the increment and, for each value, the IRI index is calculated using Proval® software. For the left side, IRI index to the TRP is 5.82 ± 0.04 m/km (class 2 – Tab. 2).

$$y = 12.05\sin(0.34t) + 12.05\cos(0.102t) \tag{3}$$

For the right side the same approach is applied, but A_1 and A_2 in Eq. (2) is established as 8.53 mm. The interval for the frequencies w_1 and w_2 taken as $(0.3:0.01:0.54)$ and, the IRI index to the TRP is 6.76 ± 0.04 m/km (class 3 – Tab. 2). Equation (4) depicts the equation:

$$y = 8.53\sin(0.54t) + 8.53\cos(0.162t) \tag{4}$$

Figure 5 illustrates the load profiles (TRP) obtained from Eq. (3) and Eq. (4). Notice that if the frequencies of both sine and cosine functions were the same, the total amplitude of Eq. (3) or Eq. (4) could be calculated by the root squared of the sum of the squared of A_1 and A_2. However, the frequencies of sine and cosine functions in Eq. (3) and (4) are different, as well as the amplitudes. Thus, the amplitude of the function expressed in each equation is a composition of each sine and cosine function at a specific time. The *S-N* diagrams to upper and lower control arms considering Eq. (3) and (4) are shown in section 4.

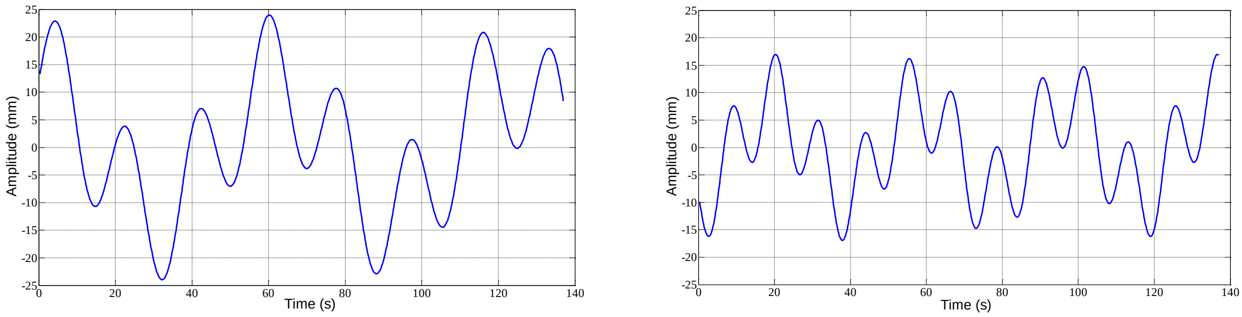

(a) (b)

Figure 5. Theoretical load profile – TRP (a) left (b) right

4. PRELIMINARY RESULTS AND DISCUSSION

Figures 6 and 7 depict the results obtained from using Eq. (3) and Eq. (4). Note that the TRP curves tend to be above the ERP curves showing, clearly, an unsafe behavior. However, the present methodology contributes to the construction of a simpler road profile, which can be easily reproduced in fatigue experimental tests, because it needs only a harmonic signal generator. Furthermore, it can be seen that above 10^6 cycles (high-cycle fatigue) the theoretical and experimental curves converge as shown in Fig. 6 (b) and Fig. 7 (b), i. e., the lower and upper control arm in the right side.

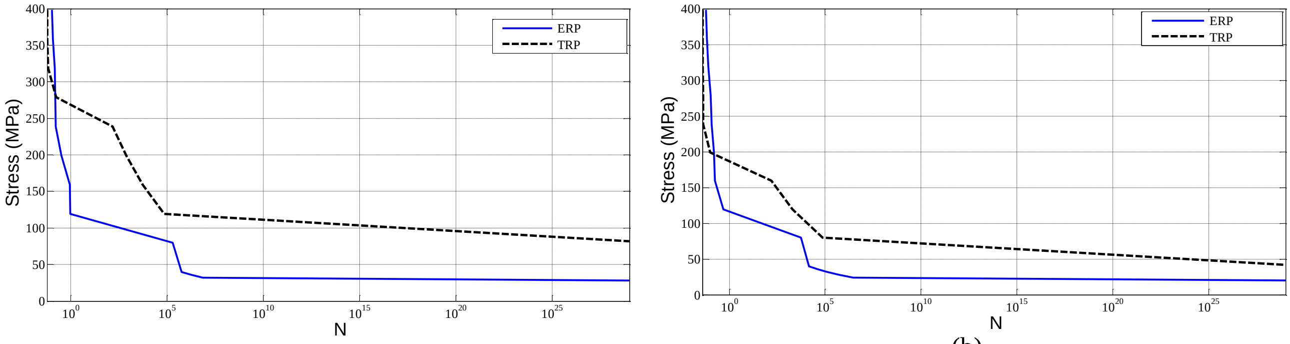

(a) (b)

Figure 6. SN diagrams for the lower control arm ERP and TRP (a) left (b) right

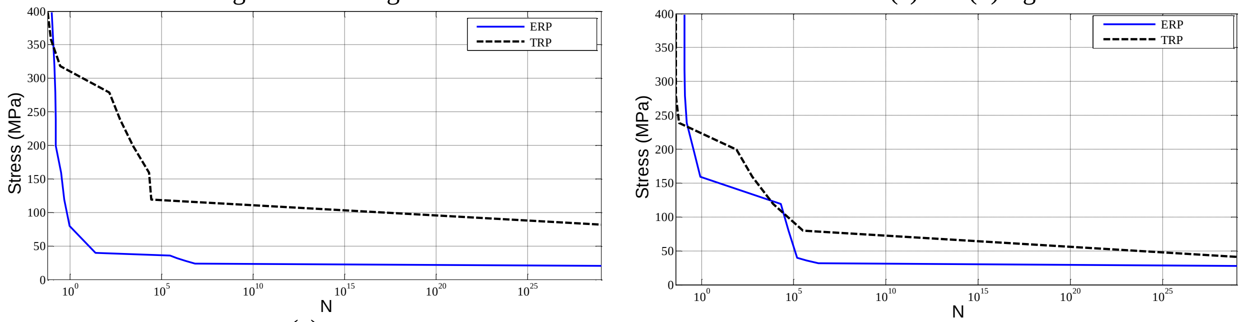

(a) (b)

Figure 7. SN diagrams for the upper control arm ERP and TRP (a) left (b) right

It can be seen from Fig. 6 and 7 a set of fatigue stresses corresponding to a fatigue cycle number lower than 10^0 cycle. In fact for a variable amplitude loading represented by the ERP (Fig. 2), some amplitude of the road profile can cause a stress, which overcome the fatigue strength defined in Eq. (1). Actually, it represents a fraction of a complete cycle (10^0).

As future works, it is proposed to use the response surface methodology (RSM) considering as boundary conditions Eq. (3) and (4) and the IRI's mean values, respectively. As preliminary result, Fig. 8 depicts the *S-N* diagram for the upper control arm submitted to the left ERP and TRP. At this point, graphs Fig. 7 (a) and Fig. 8 are comparable; EPR curve is the same, but the TRP at Fig. 8 is below the ERP curve keeping a safety behavior. IRI value for the TRP continues in the same class 2 – Tab. 2. Differences between the two curves should be investigated, but curves are very close in the high-cycle fatigue.

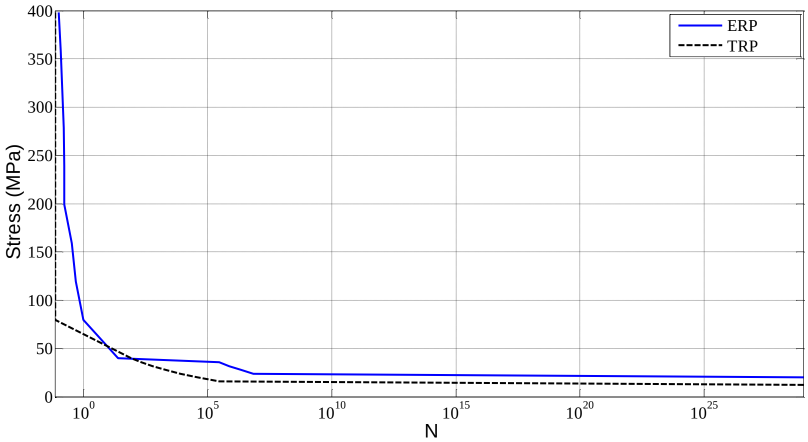

Figure 8. SN diagram for the upper control arm ERP and TRP left using RSM methodology

5. CONCLUSION

From the preliminary results obtained by the proposed methodology, it seems that the authors find a suitable way to represent random road profile in sine shape, in order to study experimentally or numerically fatigue lyfe in suspension components. The methodology considered the amplitude value corresponding to the highest occurrence value to construct the TRP functions and, the IRI index to classify, because according to the literature it is the most used roughness index for characterizing a pavement quality.

According to the preliminary results, the use of the RSM can contribute to the study representing a good tool to optimize the TRP.

6. ACKNOWLEDGEMENTS

The authors would like to thanks DPP/UnB (Decanato de Pesquisa e Pós-Graduação da Universidade de Brasília) for the support given to develop the research at the University.

7. REFERENCES

ASTM International, designation E 1926 – 08. “Standard practice for computing International Roughness Index of roads from longitudinal profile measurements”, 2014.

ASTM International, designation E 1364 – 95. “Test method for measuring road roughness by static level method”.

Chang, J. R. *et al*, 2009. “Measurement of the international roughness index (IRI) using an autonomous robot (P3-AT)”. In *Proceedings of the 26th International Symposium on Automation and Robotics in Construction – ISARC 2009*, Austin, Texas.

Committee of Transport Officials – COTO. *Guidelines for Network Level Measuremanet fo Road Roughness*. South Africa.

Departamento Nacional de Estradas de Rodagem – DNER. *Calibração e controle de sistemas medidores de irregularidades de superfície de pavimento*. Pro 164/94, p. 01/18.

D’Ippolito, R. *et al*, 2009. “Improving the fatigue life of a vehicle knuckle with a reliability-based design optimization approach”. *Journal of Statistical Planning and Inference*, Vol. 139, p. 1619-1632.

Fourlaris, G. Ellwood, R. and Jones, T. B., 2006. “The reliability of test results from simple test samples in predicting the fatigue performance of automotive components”. *Materials and Design*, Vol. 28, p. 1198-1210.

Gillespie, T. D., 1992. “Fundamentals of vehicle dynamics”. SAE – Society of Automotive Engineers.

Reimpell, J., Stoll, H. and Betzler, J. W., 2001. “The automotive chassis: engineering principles”. Butterworth Heinemann, 2nd edition.

Ren, X. D. et al, 2012. “A model for reliability and confidence level in fatigue statistical calculation”. *Theoretical and Applied Fracture Mechanics*, Vol. 59 p. 29-33.

Santos, M. A. A., 2012. *Simulação numérica dos efeitos de cargas dinâmicas na vida de fadiga de pavimentos.* Ph. D. Thesis, Universidade de Brasília, Brasilia, Brazil.

Shigley, J. E., Mischke, C. R. and Budynas, R. G., 2008. Mechanical Engineering. McGraw-Hill, 8nd edition.

Song, C. Y. and Lee, J., 2011. “Reliability-base design optimization of knuckle component using conservative method of moving least squares meta-models”. *Probabilistic Engineering Mechanics*, Vol. 26, p. 364-379.

Suresh, S., 1998. Fatigue of Materials. Cambridge University Press, 2nd edition.

Zografos, A., Dini, D., Olver, A. V., 2009. “Freeting fatigue and wear in bolted connections: A multi-level formulation for the computation of local contact stress”. *Tribology International*, Vol. 42, p. 1663-1675.

8. RESPONSIBILITY NOTICE

The authors are the only responsible for the printed material included in this paper.